MECHANICAL DESIGN AND STRUCTURAL ANALYSIS OF SEPTUM MAGNET FOR THAILAND NEW SYNCHROTRON LIGHT SOURCE (SPS-II)

K. Phochanasombut*[1], N. Chaijaroenmaitree[1], S. Morakul[1]
T. Leetha[2], T. Phimsen[2], P. Sunwong[2], T. Yan[2]
[1]Chulalongkorn University, Bangkok, Thailand
[2]Synchrotron Light Research Institute, Nakhon Ratchasima, Thailand

Abstract

The Synchrotron Light Research Institute of Thailand is developing a new eddy-current septum magnet as part of the pulsed magnet systems for its next-generation synchrotron light source, the Siam Photon Source II (SPS-II). This work focuses on mechanical design and structural analysis of the septum magnet to improve the prediction of anomalies and potential failures over the machine's operational lifetime. The finite element method is used to evaluate both the static deformation of the in-air magnet yoke and the transient vibration response of the septum blade under pulsed magnetic force, which can induce fatigue damage through cumulative stress cycles. Static analysis indicates that the proposed design satisfies the structural integrity and magnetic field uniformity requirements. The impulse vibration fatigue assessment of the septum blade falls within the ultra-high-cycle fatigue (UHCF) regime, with established S–N data for copper alloys providing design guidance for extending the magnet's operational life.

INTRODUCTION

The development of the Siam Photon Source II (SPS-II) represents a major advancement in scientific infrastructure in Southeast Asia, with the potential to significantly enhance research and innovation capabilities across the region. As a next-generation synchrotron facility, SPS-II will offer higher energy and higher intensity photon beams with improved beam characteristics compared to the existing Siam Photon Source (SPS). It will play a significant role in supporting Thailand, as well as other ASEAN countries, in the transition to a research and innovation-driven economy [1].

SPS-II will consist of three accelerating structures: the linear accelerator (LINAC), the booster synchrotron, and the storage ring synchrotron. Beam transfer between accelerators requires injection and extraction systems designed to minimize beam loss; a combination of septa and kicker magnets is frequently used for these applications.

A septum separates two field regions: one with a homogeneous field for deflecting the beam, and the other with a low fringe field so as not to affect the circulating beam, providing spatial separation of the circulating and injected/extracted beams [2]. This research focuses on the eddy-current septum, powered with a half or full sine wave current pulse to create a fast-rising magnetic field. When pulsed, eddy currents induced in the septum counteract the fringe field. The operational magnet is subjected to static and dynamic forces that can cause deformation and alter its electromagnetic properties, motivating mechanical stress–strain and impulse vibration analysis using the finite element method (FEM).

* kantanat.pho@gmail.com

LITERATURE REVIEW

Eddy-current septum magnets maintain very thin effective septa of 1 mm to 3 mm with unconstrained coil dimensions [2]. They have been developed in many accelerators, such as the SOLEIL synchrotron [3], the SSRF storage ring [4], the CERN SPS [5], and J-PARC [6, 7]. Studies on the MSe1 septum magnet [8] showed that finite element optimization with reinforcement plates significantly reduced stress concentrations at the coil–conductor interface. At CERN, high-fidelity modelling and vibration monitoring of pulsed septa demonstrated the importance of modal and transient response simulations in predicting fatigue life [9].

Various methods exist to characterise vibration fatigue in both the time and frequency domains [10–12]. The rainflow counting method is widely regarded as the most accurate cycle-counting algorithm for variable amplitude and random loadings, extracting cycles based on material memory mechanisms introduced through the "pagoda-roof" method. Several formulations have been developed, including the ASTM "3-points" algorithm [13], the "4-points" algorithm [14], and Rychlik's non-recursive formulation [15]. Identified cycle amplitudes are used with the Palmgren–Miner linear damage rule [16].

Ultra-high-cycle fatigue (UHCF) [17–19], defined as the regime beyond 10^8 cycles and extending to 10^{10} or more, is crucial for copper alloys in accelerator applications. Investigations for CLIC structures with a design lifetime of 2.33×10^{10} cycles [20, 21] established that pure copper (C10100) in a 50 % cold-worked state exhibits only 110 MPa fatigue strength at 10^{10} cycles, while precipitation-hardened CuZr (C15000) achieved 180 MPa and GlidCop Al-15 (C15715) reached 160 MPa.

METHODOLOGY

Static Structural Analysis

A static structural analysis was conducted in ANSYS using the plane-strain assumption, which is valid here because the yoke length along z greatly exceeds the in-plane dimensions,

the laminated plates are constrained in z by preloaded bolts, and the primary magnetic forces act in the xy-plane. The out-of-plane strain is therefore negligible:

$$\varepsilon_z = \frac{1}{E}[\sigma_z - \nu(\sigma_x + \sigma_y)] = 0\,. \tag{1}$$

Geometric Model and Design Reference The geometric profile was based on the initial design specifications of the first Thai synchrotron septum magnet, enhanced with a fixed housing condition and frictionless contact behaviour at all magnet-to-support interfaces. The schematic drawing and CAD model are shown in Figs. 1 and 2.

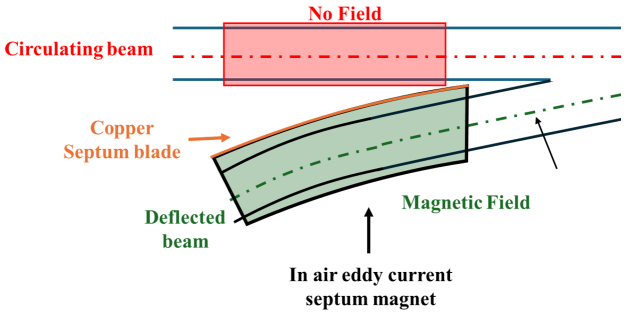

Figure 1: Schematic drawing of the septum magnet.

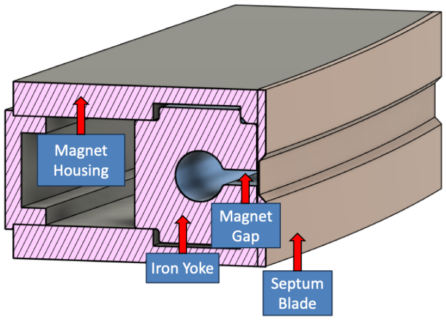

Figure 2: CAD model of the septum magnet.

Boundary Conditions and Loading The electromagnetic force across the gap was calculated as

$$F = \frac{B^2 S}{2\mu_0} \approx 8\,\text{kN}\,, \tag{2}$$

with $B = 0.9\,\text{T}$ over gap surface S. Normalised by the yoke length of 1.2 m, this gives a distributed line load of 6.667 N/m (Forces A and B in Fig. 3). Standard gravity was applied at the yoke centre of mass (Force D), and a fixed-support constraint was applied to the bottom surface of the housing (Label C).

Material Properties The yoke was modelled as non-oriented electrical steel (NOES), a low-carbon steel with 2 % to 4 % silicon content. Material parameters are given in Table 1 [22, 23].

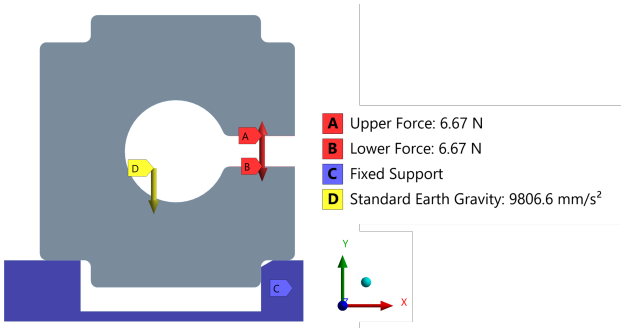

Figure 3: Boundary conditions applied in the static analysis.

Table 1: Material Properties of the Septum Magnet Yoke

Material	ν	E [GPa]	ρ [kg/m^3]	σ_y [MPa]
NOES	0.29	195	7700	450

Vibration Fatigue Analysis

The septum blade (curvature radius 3333 mm, arc 15°) was modelled in two FE configurations: a 2D plane model (0.2 mm 6-node triangular elements; 26 964 nodes) and a 3D solid model (1.0 mm 20-node hexahedra; 140 998 nodes). Material parameters are listed in Table 2. Modal analysis was followed by Mode Superposition (MSUP) transient simulation using $\zeta = 0.02$ (from impact vibration testing), a 10 µs time step, and two consecutive half-sine force pulses (first peak 4.5 N/mm, second reduced by 20 %) applied at the blade centre, repeating every 200 ms.

Table 2: Material Properties of the Septum Blade

Material	ν	E [GPa]	ρ [kg/m^3]	σ_y [MPa]
Copper	0.34	110	8300	313

The resulting von Mises stress history was processed in MATLAB through three steps: (i) rainflow cycle counting per ASTM E1049 [13], extracting amplitude–mean pairs (S_a, S_m); (ii) mean stress correction using uncorrected, modified Goodman (Eq. (3)), and Gerber (Eq. (4)) criteria with $S_{ut} = 360$ MPa; and (iii) Palmgren–Miner damage summation (Eq. (5)) against the UHCF S–N curve ($S_e = 105$ MPa), with failure at $D = 1.0$ and life $= T_{\text{block}}/D$.

$$S_{a,\text{eq}} = \frac{S_a}{1 - S_m/S_{ut}}\,, \tag{3}$$

$$S_{a,\text{eq}} = \frac{S_a}{1 - (S_m/S_{ut})^2}\,, \tag{4}$$

$$D = \sum_{i=1}^{k} \frac{n_i}{N_{f,i}}\,. \tag{5}$$

RESULTS

Static Structural

The maximum von Mises stress was 4.5 MPa at the C-shaped inner boundary (Fig. 4), far below the NOES yield strength of 450 MPa. Normal and shear stress distributions

show σ_y peaked along the vertical plane of symmetry, with localised concentrations in σ_x and τ_{xy} at the shoulder fillets, indicating the fillet radius is a critical geometric parameter.

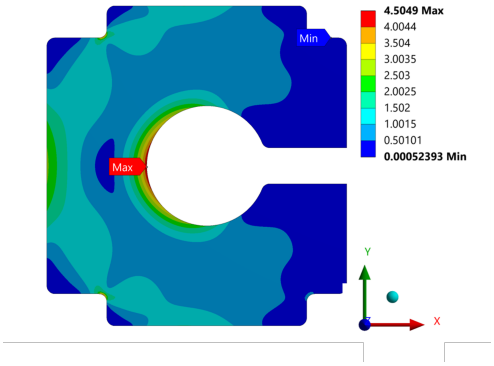

Figure 4: Von Mises stress distribution (MPa) in the septum magnet yoke.

The maximum vertical deformation δ_y at the upper pole reached 4.703 µm at the right tip, decreasing to 3.077 µm at the left (Fig. 5). The lower surface showed a maximum of 0.104 µm, the asymmetry arising from the structural overhang of the upper assembly. All values remain within manufacturing tolerances.

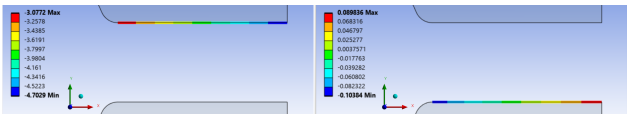

Figure 5: Vertical deformation (y-direction, µm) of upper and lower poles.

Vibration Fatigue

Both models confirmed full attenuation within the 200 ms pulse interval, indicating no resonance build-up. The 3D centreline deformation peaked at 0.057 mm then decayed gradually; the 2D model showed a lower peak of 0.046 mm with faster decay. Peak von Mises stresses of 106 MPa (3D, at the bolt hole) and 125 MPa (2D, at the fixed support) transiently exceeded S_e = 105 MPa. However, rainflow processing of the stress history (Fig. 6) showed that all extracted cycles fell in the low-S_m, low-S_a region, well below the Goodman, Gerber, and uncorrected endurance limit boundaries. Consequently, no cycles contributed to fatigue damage under the Palmgren–Miner framework, yielding an effectively infinite fatigue life for both models.

DISCUSSION

The plane-strain assumption is justified by the z-axis bolt preload and in-plane force application. Although NOES is anisotropic, orthotropic and isotropic results show no significant differences in this configuration; the isotropic assumption was therefore adopted. The maximum static stress (4.5 MPa) is well below the yield strength (450 MPa), confirming structural safety. Shoulder fillet optimisation could further reduce localised concentrations. The upper-to-lower pole deformation asymmetry arises from the structural

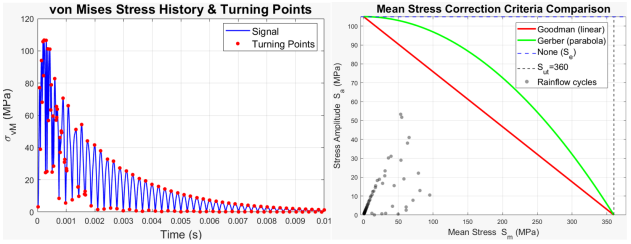

(a) 3D model

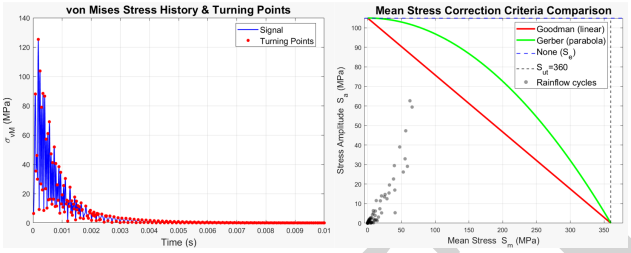

(b) 2D model

Figure 6: Von Mises stress history with turning points (left) and mean stress correction diagram with rainflow cycles (right).

overhang; improved support alignment could prevent long-term drift and magnetic field degradation.

Although the instantaneous peak stress transiently exceeded S_e, all rainflow cycle amplitudes remained within the safe-life region, yielding zero total Miner's damage. The 3D model is the more representative configuration, capturing out-of-plane bending and torsional contributions that the 2D model excludes; their agreement on infinite fatigue life provides additional confidence in the design.

CONCLUSION

This study presented the mechanical design and structural analysis of an eddy-current septum magnet for SPS-II using a comprehensive FEM framework. Static analysis confirmed that all stress magnitudes remain well below material yield limits and deformations are within tolerances for magnetic field quality. Using $\zeta = 0.02$ from impact vibration testing, MSUP transient simulation confirmed dynamic decay within 0.01 s, well within the 200 ms pulse interval. Rainflow cycle counting and mean stress correction yielded zero cumulative damage and effectively infinite fatigue life. The 3D model was identified as the more representative configuration. Future work will focus on fillet radius optimisation and experimental validation through modal testing and strain measurements.

REFERENCES

[1] P. Klysubun *et al.*, "SPS-II: a 4th generation synchrotron light source in Southeast Asia", in *Proc. IPAC'22*, Bangkok, Thailand, Jun. 2022, pp. 847–850. doi:10.18429/JACoW-IPAC2022-MOOPLGD2

[2] M. J. Barnes, J. Borburgh, B. Goddard, and M. Hourican, "Injection and extraction magnets: septa", in *Proc. CERN Accelerator School: Magnets*, Bruges, Belgium, Jun. 2009, pp. 167–184. doi:10.5170/CERN-2010-004.167

[3] C. Prior, Ed., "Proc. epac'06" (Edinburgh, UK, Jun. 26–30, 2006), European Particle Accelerator Conference 10, JACoW Publishing, Geneva, Switzerland,

[4] W. Kang *et al.*, "Design of the SSRF septum magnets", in *Proc. APAC'01*, Beijing, China, Sep. 2001, pp. 663–665.

[5] G. H. Schröder *et al.*, "Injection and extraction magnets: septa", in *Proc. EPAC'00*, Vienna, Austria, Jun. 2000, pp. 2370–2372.

[6] K. Fan, K. Ishii, H. Matsumoto, N. Matsumoto, T. Shibata, and T. Sugimoto, "New design of J-PARC main ring injection system for high beam power operation", in *Proc. IPAC'14*, Dresden, Germany, Jun. 2014, pp. 2097–2099. doi:10.18429/JACoW-IPAC2014-WEPRO065

[7] T. Shibata *et al.*, "The development of a new low-field septum magnet system for fast extraction in the main ring of J-PARC", *J. Phys.: Conf. Ser.*, vol. 1067, p. 052020, Sep. 2018. doi:10.1088/1742-6596/1067/5/052020

[8] Y. Wei *et al.*, "Structure parametric optimization and mechanical analysis of the MSe1 septum magnet", *IEEE Trans. Appl. Supercond.*, vol. 34, no. 5, pp. 1–5, Aug. 2024. doi:10.1109/TASC.2024.3369008

[9] K. Kawa, T. Szumlak, C. Kokkinos, and F. Lackner, "High fidelity numerical modelling and condition monitoring applied to septum magnets at CERN", in *Proc. IPAC'24*, Nashville, TN, USA, May 2024, pp. 3556–3559. doi:10.18429/JACoW-IPAC2024-THPR29

[10] P. Ogrinec, J. Slavič, M. Česnik, and M. Boltežar, "Vibration fatigue at half-sine impulse excitation in the time and frequency domains", *Int. J. Fatigue*, vol. 123, pp. 308–317, Jun. 2019. doi:10.1016/j.ijfatigue.2019.02.031

[11] F. Li, H. Wu, and P. Wu, "Vibration fatigue dynamic stress simulation under non-stationary state", *Mech. Syst. Signal Process.*, vol. 146, p. 107006, Jan. 2021. doi:10.1016/j.ymssp.2020.107006

[12] J. Sun, A. Baktheer, Y. Pan, and F. Aldakheel, "Fatigue life prediction under random vibrations: an acceleration framework combining scale factor analysis and critical distance theory", *Theor. Appl. Fract. Mech.*, vol. 140, p. 105108, Dec. 2025. doi:10.1016/j.tafmec.2025.105108

[13] ASTM International, "Standard practices for cycle counting in fatigue analysis, ASTM e1049-85", ASTM International, West Conshohocken, PA, USA, 1985,

[14] C. Amzallag, J. P. Gerey, J. L. Robert, and J. Bahuaud, "Standardization of the rainflow counting method for fatigue analysis", *Int. J. Fatigue*, vol. 16, no. 4, pp. 287–293, Jun. 1994. doi:10.1016/0142-1123(94)90343-3

[15] I. Rychlik, "A new definition of the rainflow cycle counting method", *Int. J. Fatigue*, vol. 9, no. 2, pp. 119–121, Apr. 1987. doi:10.1016/0142-1123(87)90054-5

[16] M. A. Miner, "Cumulative damage in fatigue", *J. Appl. Mech.*, vol. 12, no. 3, A159–A164, Sep. 1945. doi:10.1115/1.4009458

[17] H. Mughrabi, "On life-controlling microstructural fatigue mechanisms in ductile metals and alloys in the gigacycle regime", *Fatigue Fract. Eng. Mater. Struct.*, vol. 22, no. 7, pp. 633–641, Jul. 1999. doi:10.1046/j.1460-2695.1999.00186.x

[18] H. Mughrabi, "Specific features and mechanisms of fatigue in the ultra high cycle regime", *Int. J. Fatigue*, vol. 28, no. 11, pp. 1501–1508, Nov. 2006. doi:10.1016/j.ijfatigue.2005.05.018

[19] S. Stanzl-Tschegg, H. Mughrabi, and B. Schönbauer, "Life time and cyclic slip of copper in the VHCF regime", *Int. J. Fatigue*, vol. 29, no. 9–11, pp. 2050–2059, Sep. 2007. doi:10.1016/j.ijfatigue.2007.03.010

[20] S. Heikkinen, "Thermally induced ultra high cycle fatigue of copper alloys of the high gradient accelerating structures", Ph.D. thesis, Aalto Univ., Espoo, Finland, 2010. https://repository.cern/records/khvgb-eda38

[21] M. Li and S. J. Zinkle, "Physical and mechanical properties of copper and copper alloys", in *Comprehensive Nuclear Materials*", in ed. by R. J. M. Konings, vol. 4, Amsterdam, The Netherlands: Elsevier, 2012, pp. 667–690, doi:10.1016/B978-0-08-056033-5.00122-1,

[22] O. Hubert, L. Daniel, and R. Billardon, "Experimental analysis of the magnetoelastic anisotropy of a non-oriented silicon iron alloy", *J. Magn. Magn. Mater.*, vol. 254–255, pp. 352–354, Jan. 2003. doi:10.1016/S0304-8853(02)00850-8

[23] C. Backes, M. Smaga, and T. Beck, "Mechanical and functional fatigue of non-oriented and grain-oriented electrical steels", *Int. J. Fatigue*, vol. 186, p. 108410, Sep. 2024. doi:10.1016/j.ijfatigue.2024.108410